A probabilistic approach for damping identification considering uncertainty in experimental modal analysis

Sifeng Bi*, Morvan Ouisse†, Emmanuel Foltête‡

Univ. Bourgogne Franche-Comté, Femto-ST Institute, CNRS/UFC/ENSMM/UTBM, 25000 Besancon-FR

The system identification technology is essentially an inverse procedure, starting from the experimentally measured response, to construct mass, stiffness, and damping matrices of the structure. However, the measurement inevitably contains uncertainties, which significantly impact the identified system characteristics, especially for damping terms. In the presence of experimental uncertainty, the aim of damping identification in this paper is not a single deterministic solution with maximum fidelity to a single experiment, but rather a set of optimized solutions with acceptable robustness to multiple uncertain experiments. To achieve this objective, an integrated approach combining deterministic identification and probabilistic calibration techniques is proposed. This approach starts from the properness condition of modes in a deterministic identification. A probabilistic estimation technique is performed on the preliminary identified data so that an uncertainty boundary is available for the calibration procedure where the genetic algorithm and classical optimization techniques are utilized. A comprehensive comparison metric for two continuous quantities is proposed as the objective function in the calibration procedure. Finally, a probabilistic validation metric is proposed to assess the stability of the calibrated damping matrix. In both simulated and experimental examples, the finally obtained matrices exhibit their robustness with regard to the experimental uncertainty.

Nomenclature

A = Integrated matrix of mass and stiffness in state-space representation

C = Damping matrix

$\mathbf{E}_n$ = $n \times n$ identity matrix

$\mathbf{F}(t)$ = Force vector in state-space representation

$\mathbf{f}(t)$ = Force vector

$\mathbf{H}(\omega)$ = Frequency response function (FRF) at the frequency point ω

K = Stiffness matrix

* Post-doc research fellow, Department of Applied Mechanics, sifeng.bi@femto-st.fr

† Professor, Department of Applied Mechanics

‡ Professor, Department of Applied Mechanics

$\mathbf{M}$ = Mass matrix

$\mathbf{U}$ = Integrated matrix of mass and damping in state-space representation

$\boldsymbol{u}$ = Column vector containing discrete experimental FRF

$\boldsymbol{v}$ = Column vector containing discrete simulated FRF

$\mathbf{\Gamma}$ = Eigenvalue matrix in state-space representation

$\mathbf{\Theta}$ = Eigenvector matrix in state-space representation

$\mathbf{\Lambda}$ = Eigenvalue matrix

λ = Single eigenvalue

μ = Mean of the matrix element

$\mathbf{\Xi}$ = arbitrary diagonal matrix

σ = Standard deviation of the matrix element

$\mathbf{\Upsilon}$ = Lagrange multiplier matrix

$\mathbf{\Phi}$ = Eigenvector matrix

φ = Single eigenvector

Subscripts

i = Index of degree of freedom

m = Number of experiments

N = Number of frequency points

n = Number of degree of freedom

p = Proper data after deterministic identification

I. Introduction

The knowledge of mass, stiffness, and damping matrices of a structural system is of first interest for the engineers to analyze, predict, and control the system behavior. Especially, damping identification has long been a popular but challenging issue because of its complex mechanisms. A precise representation of damping is critical for active vibration control in fields such as aerospace, automobile, and civil engineering. Considering the inevitable uncertainties in engineering, this paper focuses on a probabilistic approach of damping identification and calibration.

Compared with the mass and stiffness, the damping identification is more difficult mainly due to the fact that no explicit theoretical model of damping mechanism is generally accepted [1]. Besides the mostly classical viscous damping proposed by Rayleigh [2], various damping models are investigated in literature, such as nonlinear viscous damping [3,4], material damping [5,6], frictional damping [7,8], and non-proportional damping [9,10]. Regardless of which damping model is proposed, an increasingly popular tendency of damping identification is to start from the complex modes [11,12], which are extracted from the measured frequency response function (FRF). Furthermore, some techniques are developed to identify the damping matrix directly from the measured FRF [13,14].

However, the above tendency raises another challenging feature, i.e. the fact that the damping term is much more sensitive to the environment noise and experimental uncertainty, compared with the mass and stiffness terms. The uncertainties, unfortunately, are inherent throughout real-life vibration experiments due to the following factors:

- *Uncertainties associated to sensors*. The accelerometers stuck on the structure unavoidably change the mass properties of the structure. Low weight sensors or non-contact technique, e.g. laser vibrometry, may be used to minimize the impact of adding mass, but even in the case of non-contact measurements, additional uncertainties are involved in various aspects of the acquisition process such as sensor sensitivity, measuring range, environment noise, and electronic signal processing.
- *Uncertainties on the excitation*. Considering a hammer excitation, the hard-to-control random effects, e.g. position, direction, and magnitude of the hammer impact, make the measurements only partially reproducible. When a shaker is utilized, different excitation waveforms, e.g. white noise and sweep sine, may lead to discrepant responses of the structure.
- *Uncertainties on the boundary conditions*. For a fixed condition, the interaction between the test object and the fixing base cannot be completely avoided because the fixing base is not ideally rigid. Alternatively, free-free conditions are difficult to handle, low stiffness supports may change the dynamical behavior of the structure, in particular in the low frequency range.
- *System errors and subjective judgements*. The computation of the FRFs from time signals are impacted by the electronic systems, the choice of windowing techniques and estimators used in the process. The complex modes are influenced by the subjective judgement of the engineer during the extracting process from the FRFs to the complex modes.

Clearly, damping identification is further muddied by experimental uncertainties. It is demonstrated in the following examples (Sections III and IV) that even slight difference among repeated measurements leads to significant discrepancy among the identified damping matrices. If the identification approach stops at these inconstant results, the engineer can only arbitrarily adopt a result from a single experimental case, which may lead to serious consequences in practical applications.

Despite the vast literature on damping identification, the published research discussing the role of uncertainties has been quite limited to the authors' knowledge. Adhikari [15] proposes approaches to quantify the damping model uncertainty, which belongs to the general category of *epistemic uncertainty* caused by the lack of knowledge regarding damping mechanism. While the experimental uncertainty considered herein refers to another general category as *aleatoric uncertainty* which is due to the inherent variability in the real-life engineering system. Koruk and Sanliturk [16] investigate the uncertainty arising from the signal processing, i.e. the exponential windowing, when measuring the FRF, and then assess different estimating method with the purpose to reduce the damping uncertainty. Both of the above-mentioned works focus on the quantification approach for a specific paradigm of uncertainty, while the inherent experimental uncertainty's influence on the final identified damping matrix is currently not addressed.

Consequently, the main aim of this work is to identify and calibrate the mass, stiffness, and especially damping matrices from the measured FRF, with the emphasis on the robustness with regard to experimental uncertainty. As the first step, the preliminary matrices are identified through the experimental modal analysis along with the so-called *properness condition* of the complex modes. In a deterministic sense, Balmès [11] proposes a valuable method to enforce the properness condition, and

this method has recently been extended to non-symmetrical problems [17] and vibroacoustical applications [18]. This deterministic approach has good performances on mass and stiffness identification, however, the precision of damping is significantly influenced by the experimental uncertainty. Consequently, Balmès' method is utilized in this paper as the initial step to generate the preliminary matrices, and a further probabilistic calibration procedure is proposed to handle the experimental uncertainty. The calibration procedure is essentially an optimization problem which should be appropriately configured from two aspects: 1) the uncertainty boundary and 2) the objective function. The uncertainty boundary is defined by a probabilistic estimation technique under a Gaussian distribution assumption. Only a small number of experiments is sufficient for this technique to objectively determine the uncertainty boundary, which can be utilized as constraints in the optimization. The objective function is defined by quantifying the difference between the measured FRF and the simulated FRF. Two correlation conceptions, namely the signature assurance criterion (SAC) and cross signature scale factor (CSF), are utilized to construct the objective function. In order to solve the optimization problem, an integrated application of the genetic algorithm and classical constrained minimization is proposed with the purpose of searching the global solution with a high precision. Finally, the mean coefficient of variation (MCV) is proposed as the validation matric to assess the stability of damping matrices. This overall approach is investigated in both numerical and experimental examples where the finally obtained damping matrix is steady and robust with regard to the experimental uncertainty.

This paper is organized as follows. Section II.A recalls the deterministic identification together with the properness enforcement method. Section II.B elaborates the probabilistic calibration procedure from four aspects, i.e. the uncertain boundary, the objective function, the optimization tools, and the validation metric. A detailed flowchart of the overall deterministic identification and probabilistic calibration approach is also presented. A numerical example is given in Section III to explain each aspect of the overall approach in detail, so that the reader can reproduce the result. Section IV presents a specially designed experimental example where multiple experiments are repeated on the same structure, but in different manners. The example provides quite interesting results as the finally obtained system matrices are steady even though the reference FRFs among the various cases are different. It clearly demonstrates the feasibility of the damping identification approach, in the presence of experimental uncertainties. Key conclusions and perspectives of this work are summarized in Section V.

II. Theories and methods

A. Deterministic identification procedure

The equation of motion of a structural system with viscous damping is classically expressed as

$$\mathbf{M}\ddot{\mathbf{q}}(t) + \mathbf{C}\dot{\mathbf{q}}(t) + \mathbf{K}\mathbf{q}(t) = \mathbf{f}(t) \tag{1}$$

Where $\mathbf{q}(t)$ is the displacement of the structure; $\mathbf{f}(t)$ is the exciting force; $\mathbf{M}, \mathbf{C}, \mathbf{K}$ are respectively the mass, damping, and stiffness matrices. The state-space representation of Eq. (1) is defined as follows:

$$\mathbf{U}\dot{\mathbf{Q}}(t) - \mathbf{A}\mathbf{Q}(t) = \mathbf{F}(t) \tag{2}$$

where

$$\mathbf{U}=\begin{bmatrix}\mathbf{C} & \mathbf{M}\\ \mathbf{M} & \mathbf{0}\end{bmatrix},\ \mathbf{A}=\begin{bmatrix}-\mathbf{K} & \mathbf{0}\\ \mathbf{0} & \mathbf{M}\end{bmatrix},\ \mathbf{Q}(t)=\begin{Bmatrix}\mathbf{q}(t)\\ \dot{\mathbf{q}}(t)\end{Bmatrix},\ \mathbf{F}(t)=\begin{Bmatrix}\mathbf{f}(t)\\ 0\end{Bmatrix}. \tag{3}$$

Let n denotes the number of Degrees of Freedom (DOF) of the physical system, the second order eigenvalue problem of Eq. (1) is expressed as

$$(\mathbf{M}\lambda_i^2+\mathbf{C}\lambda_i+\mathbf{K})\boldsymbol{\varphi}_i=0 \qquad i=1,2,\dots,n \tag{4}$$

where λ_i and $\boldsymbol{\varphi}_i$ are respectively the i-th eigenvalue and eigenvector. Let $\boldsymbol{\theta}_i=\begin{bmatrix}\boldsymbol{\varphi}_i\\ \boldsymbol{\varphi}_i\lambda_i\end{bmatrix}$, the corresponding state-space representation of the eigenvalue problem is

$$(\mathbf{U}\lambda_i-\mathbf{A})\boldsymbol{\theta}_i=0 \ \text{ and } \ (\mathbf{U}\overline{\lambda_i}-\mathbf{A})\overline{\boldsymbol{\theta}_i}=0 \tag{5}$$

where $\overline{\blacksquare}$ denotes the conjugate of the complex mode. The matrix form containing all of the n eigenvalues and eigenvectors is assembled as

$$\boldsymbol{\Lambda}=\begin{bmatrix}\ddots & & \\ & \lambda_i & \\ & & \ddots\end{bmatrix};\ \boldsymbol{\Phi}=[\boldsymbol{\varphi}_1\ \boldsymbol{\varphi}_2\ \cdots\ \boldsymbol{\varphi}_n]. \tag{6}$$

The state-space representation of $\boldsymbol{\Lambda}$ and $\boldsymbol{\Phi}$ are respectively $\boldsymbol{\Gamma}$ and $\boldsymbol{\Theta}$ with the size as $2n\times 2n$:

$$\boldsymbol{\Gamma}=\begin{bmatrix}\boldsymbol{\Lambda} & \mathbf{0}\\ \mathbf{0} & \overline{\boldsymbol{\Lambda}}\end{bmatrix};\ \boldsymbol{\Theta}=\begin{bmatrix}\boldsymbol{\Phi} & \overline{\boldsymbol{\Phi}}\\ \boldsymbol{\Phi}\boldsymbol{\Lambda} & \overline{\boldsymbol{\Phi}\boldsymbol{\Lambda}}\end{bmatrix}. \tag{7}$$

Then Eq. (5) can be rewritten in the matrix form

$$\mathbf{U}\boldsymbol{\Theta}\boldsymbol{\Gamma}=\mathbf{A}\boldsymbol{\Theta}. \tag{8}$$

Supposing a diagonal matrix assembled by $2n$ arbitrary real values, $\boldsymbol{\Xi}=\begin{bmatrix}\ddots & & \\ & \xi_i & \\ & & \ddots\end{bmatrix}$, $i=1,\cdots,2n$, the orthogonality between each mode is expressed as

$$\boldsymbol{\Theta}^T\mathbf{U}\boldsymbol{\Theta}=\boldsymbol{\Xi} \ \text{ and } \ \boldsymbol{\Theta}^T\mathbf{A}\boldsymbol{\Theta}=\boldsymbol{\Xi}\boldsymbol{\Gamma} \tag{9}$$

where $\blacksquare^T$ is the transposition symbol. An important step herein is to normalize the eigenvector matrix $\boldsymbol{\Phi}$ so that the arbitrary diagonal matrix $\boldsymbol{\Xi}$ is transformed into a $2n\times 2n$ identity matrix. After the normalization, inverting form of Eq. (9) is expressed as

$$\mathbf{U}^{-1}=\boldsymbol{\Theta}\boldsymbol{\Theta}^T \ \text{ and } \ \mathbf{A}^{-1}=\boldsymbol{\Theta}\boldsymbol{\Gamma}^{-1}\boldsymbol{\Theta}^T. \tag{10}$$

Considering Eqs. (3) and (7), Eq. (10) can be rewritten using the terms of the n-DOF physical system:

$$\begin{aligned}\begin{bmatrix}\mathbf{C} & \mathbf{M}\\ \mathbf{M} & 0\end{bmatrix}^{-1}&=\begin{bmatrix}0 & \mathbf{M}^{-1}\\ \mathbf{M}^{-1} & -\mathbf{M}^{-1}\mathbf{C}\mathbf{M}^{-1}\end{bmatrix}=\begin{bmatrix}\boldsymbol{\Phi}\boldsymbol{\Phi}^T+\overline{\boldsymbol{\Phi}}\overline{\boldsymbol{\Phi}^T} & \boldsymbol{\Phi}\boldsymbol{\Lambda}\boldsymbol{\Phi}^T+\overline{\boldsymbol{\Phi}\boldsymbol{\Lambda}}\overline{\boldsymbol{\Phi}^T}\\ \boldsymbol{\Phi}\boldsymbol{\Lambda}\boldsymbol{\Phi}^T+\overline{\boldsymbol{\Phi}\boldsymbol{\Lambda}}\overline{\boldsymbol{\Phi}^T} & \boldsymbol{\Phi}\boldsymbol{\Lambda}^2\boldsymbol{\Phi}^T+\overline{\boldsymbol{\Phi}\boldsymbol{\Lambda}^2}\overline{\boldsymbol{\Phi}^T}\end{bmatrix}\\ \begin{bmatrix}-\mathbf{K} & 0\\ 0 & \mathbf{M}\end{bmatrix}^{-1}&=\begin{bmatrix}-\mathbf{K}^{-1} & 0\\ 0 & \mathbf{M}^{-1}\end{bmatrix}=\begin{bmatrix}\boldsymbol{\Phi}\boldsymbol{\Lambda}^{-1}\boldsymbol{\Phi}^T+\overline{\boldsymbol{\Phi}\boldsymbol{\Lambda}}^{-1}\overline{\boldsymbol{\Phi}}^T & \boldsymbol{\Phi}\boldsymbol{\Phi}^T+\overline{\boldsymbol{\Phi}}\overline{\boldsymbol{\Phi}^T}\\ \boldsymbol{\Phi}\boldsymbol{\Lambda}\boldsymbol{\Phi}^T+\overline{\boldsymbol{\Phi}}\overline{\boldsymbol{\Phi}^T} & \boldsymbol{\Phi}\boldsymbol{\Lambda}\boldsymbol{\Phi}^T+\overline{\boldsymbol{\Phi}\boldsymbol{\Lambda}}\overline{\boldsymbol{\Phi}^T}\end{bmatrix}.\end{aligned} \tag{11}$$

Clearly, the mass, damping and stiffness matrices can be constructed using the complex modes:

$$\begin{cases}\mathbf{M}=\left[\boldsymbol{\Phi}\boldsymbol{\Lambda}\boldsymbol{\Phi}^T+\overline{\boldsymbol{\Phi}\boldsymbol{\Lambda}}\overline{\boldsymbol{\Phi}^T}\right]^{-1}\\ \mathbf{C}=-\left[\mathbf{M}\left(\boldsymbol{\Phi}\boldsymbol{\Lambda}^2\boldsymbol{\Phi}^T+\overline{\boldsymbol{\Phi}\boldsymbol{\Lambda}}^2\overline{\boldsymbol{\Phi}}^T\right)\mathbf{M}\right]\\ \mathbf{K}=-\left[\boldsymbol{\Phi}\boldsymbol{\Lambda}^{-1}\boldsymbol{\Phi}^T+\overline{\boldsymbol{\Phi}\boldsymbol{\Lambda}}^{-1}\overline{\boldsymbol{\Phi}}^T\right]^{-1}.\end{cases} \tag{12}$$

The above inverse procedure is valid only if the so-called *properness condition* is satisfied, which can be easily yielded from Eq. (11):

$$\boldsymbol{\Phi}\boldsymbol{\Phi}^{\boldsymbol{T}} + \overline{\boldsymbol{\Phi}}\,\overline{\boldsymbol{\Phi}^{\boldsymbol{T}}} = 0. \tag{13}$$

In practical applications, the complex modes are extracted from the experimental measurements with inevitable noise and uncertainties. Consequently, the properness condition is generally not satisfied, implying that the complex modes cannot be directly utilized in Eq. (12). Balmès [11] proposes a method to calibrate the eigenvectors so that the properness condition is enforced. This method is employed in the deterministic identification procedure, which is simply recalled as follows.

The properness enforcement method essentially consists in finding an approximate eigenvector matrix $\widetilde{\boldsymbol{\Phi}}$, which is as close as possible to the original $\boldsymbol{\Phi}$, while to make sure $\widetilde{\boldsymbol{\Phi}}$ (and its conjugate) fulfills Eq. (13). Solution of this problem is achieved by a Lagrange multiplier matrix $\boldsymbol{\Upsilon}$:

$$\widetilde{\boldsymbol{\Phi}} = \left[\mathbf{E}_n - \boldsymbol{\Upsilon}\overline{\boldsymbol{\Upsilon}}\right]^{-1}\left[\boldsymbol{\Phi} - \boldsymbol{\Upsilon}\overline{\boldsymbol{\Phi}}\right] \tag{14}$$

where $\mathbf{E}_n$ is the $n \times n$ identity matrix. $\boldsymbol{\Upsilon}$ can be obtained by solving the Riccati equation

$$\boldsymbol{\Phi}\boldsymbol{\Phi}^{\boldsymbol{T}} - \boldsymbol{\Upsilon}\overline{\boldsymbol{\Phi}}\boldsymbol{\Phi}^{T} - \boldsymbol{\Phi}\overline{\boldsymbol{\Phi}}^{T}\boldsymbol{\Upsilon} + \boldsymbol{\Upsilon}\overline{\boldsymbol{\Phi}\boldsymbol{\Phi}}^{T}\boldsymbol{\Upsilon} = 0. \tag{15}$$

This method performs well when reconstructing the mass and stiffness matrices [18]. However, the damping matrix is always obtained with non-ignorable error, which is demonstrated in the following examples (Sections III and IV). Explanation of this phenomenon is that the properness enforced eigenvectors are not those of the original system, but the numerically approximation of the physical ones that verify the properness condition. Compared with the mass and stiffness matrices, the equation of damping matrix in Eq. (12) is more complex with a higher power of the eigenvectors, implying that the damping term is more sensitive to the imprecision of the eigenvectors. Furthermore, the above deterministic identification procedure is based on a single set of experimental FRF, implying no uncertainty is considered in this procedure.

B. Probabilistic calibration procedure

In order to improve the robustness of the identified damping matrix, i.e. to appropriately cope with the uncertainty from the experimental measurements, a further probabilistic calibration procedure is proposed following the above mentioned deterministic identification procedure. The overall approach combining the deterministic identification (Part I) and the probabilistic calibration (Part II) is illustrated in Fig. 1.

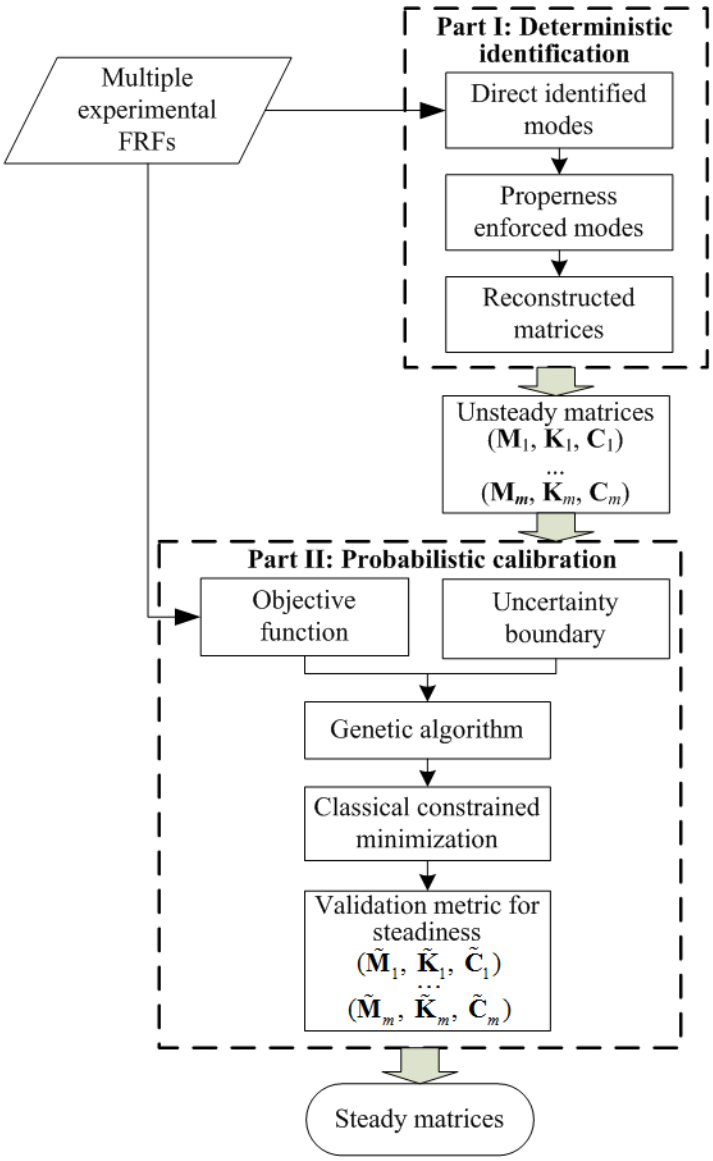

Fig. 1: Flowchart of the overall identification and calibration approach

1 Uncertainty boundary

The overall approach starts from multiple measurements where the uncertainty information is naturally involved, due to the uncertainty sources introduced in Section I. However, the uncertainty information in the original FRFs cannot be directly conducted in the calibration procedure. The first task is to transform the "gross" uncertainty information (from the original FRFs) into the explicit and processable information relative to the final objective, i.e. the system matrices. A probabilistic estimation technique is proposed to fulfill this task by determining an uncertainty boundary of the damping matrix, based on the available set of measured FRFs.

As shown in Fig. 1, each single measurement is respectively identified by the deterministic identification procedure, after which the preliminary system matrices are constructed using Eq. (12). Supposing the total number of measurements is m, the identification procedure is repeated m times and the corresponding matrices are obtained as $\mathbf{M}_1, \mathbf{K}_1, \mathbf{C}_1; \cdots; \mathbf{M}_m, \mathbf{K}_m, \mathbf{C}_m$. Note

that no uncertainty information is considered in each single execution of the identification procedure. Consequently, the matrices in each case are different from those of the other cases, even though these matrices are expected to reflect the same structure's properties. However, a cross investigation of these unsteady matrices can reveal the uncertainty information rooting in the original FRFs. It is reasonable to believe that the effective value of the matrices for a given operational experiment configuration should be within a *likely* range relative to these unsteady matrices. This range can be objectively determined in a probabilistic sense under a pre-determined confidence degree.

In the following calibration, each element of the matrices is taken as the parameter to be calibrated. Practically, the experimental repeating number *m* is always limited by time or financial burden, leading the exact distribution of the parameter population is difficult to be determined using such a limited observation sample. However, the observation sample can be used to estimate statistical features of the population via the moment estimation method [19], where the mean μ and variance σ^2 are estimated as

$$\mu = \frac{1}{m}\sum_{i=1}^{m} x_i;$$

$$\sigma^2 = \frac{1}{m-1}\sum_{i=1}^{m}(x_i - \mu)^2. \tag{16}$$

Each uncertain parameter in the damping matrix is assumed to obey the Gaussian distribution with the above estimated mean and variance. Note that, the Gaussian assumption in this specific application is supported by the justification of the central limit theorem. In this experimental damping identification process, the uncertainty of the damping matrices originates from a large number of uncertain factors in both experiment and identification steps, such as factors relative to the sensor sensitivity, boundary condition, environment noise, excitation property (i.e. position, direction, and magnitude), observational system error, and electronic signal noise, etc. According to central limit theorem, such a large number of random factors are summed up toward a Gaussian distribution. This explains why the Gaussian distribution is widely utilized in various techniques of uncertainty analysis, such as sensitivity analysis [20] and Bayesian updating [21], verification and validation [22]. However, it should be note that the Gaussian distribution is not a universal assumption for any application; in other words, an appropriate investigation on the prior data and system is required before the assumption is made.

In the Gaussian distribution, confidence bounds define the probability that a new sample will fall inside the defined uncertainty boundary. Clearly the larger boundary provides the higher probability, while also leads to more difficulty when searching the global solution in a large parameter space. In the following context, it is recommended to use the boundary with two standard deviations distance from the mean, i.e. to define the uncertainty boundary as $[\mu - 2\sigma, \mu + 2\sigma]$ such that the probability in Gaussian distribution is 95.4%.

2 Objective function

In addition to the uncertainty boundary, another critical aspect of the calibration procedure is the objective function, which can significantly influence the calibration outcomes. The final objective of this work is the system matrices of an equivalent system which can represent the same behavior as the experimental measured one. It is natural to take the system behavior, i.e. the FRF, as the reference and the difference between the experimental and simulated FRFs is used to define the objective function. Using the system matrices, the simulated FRF is calculated as

$$\mathbf{H}(\omega) = [-\mathbf{M}\omega^2 + j\mathbf{C}\omega + \mathbf{K}]^{-1}\mathbf{F} \tag{17}$$

where $\mathbf{H}(\omega)$ is the FRF at the frequency point ω; j is the imaginary unit; $\mathbf{F}$ is the identity harmonic excitation.

Supposing the number of discrete frequency points within the frequency range of interest is N, then the FRF of a n-DOF system is presented as a $n \times N$ complex matrix. Classical techniques to evaluate the difference between two complex and continuous variables are the signature assurance criterion (SAC) and cross signature scale factor (CSF) [23]. Based on the widely used modal assurance criterion (MAC) [24], SAC of the i-th DOF is defined as

$$\mathrm{SAC}^i = \frac{(\boldsymbol{u}^* \cdot \boldsymbol{v})^2}{(\boldsymbol{u}^* \cdot \boldsymbol{u})(\boldsymbol{v}^* \cdot \boldsymbol{v})} \tag{18}$$

where $\boldsymbol{u}^T = [\log \mathbf{H}_e^i(\omega_1),\ \log \mathbf{H}_e^i(\omega_2), \dots, \log \mathbf{H}_e^i(\omega_N)]$; $\boldsymbol{v}^T = [\log \mathbf{H}_s^i(\omega_1), \log \mathbf{H}_s^i(\omega_2), \dots, \log \mathbf{H}_s^i(\omega_N)]$; $\blacksquare^*$ denotes the conjugate transpose; and the superscript i is the index of DOF; the subscript e and s respectively denotes the experimental and simulated FRFs. Note that the frequency points $[\omega_1, \omega_2, \dots, \omega_N]$ are selected not only from the resonant frequency range but also from the anti-resonant frequency range, leading huge differences among the discrete FRF amplitudes. Thus it is necessary to utilize the logarithmic values of the FRF amplitudes when constructing $\boldsymbol{u}$ and $\boldsymbol{v}$, such that the weightings among FRF amplitudes under the frequency points $[\omega_1, \omega_2, \dots, \omega_N]$ can be averaged.

Consequently, the is critical such that the importance to the errors in the complete frequency range is averaged.

The SAC has a single value ranging from zero to 1, where one implies a complete correlation between the two investigated vectors. However, a drawback of SAC is revealed when the two vectors are completely proportional but with different amplitudes, i.e. $\boldsymbol{u} = \alpha \cdot \boldsymbol{v}$ where α is a non-zero real value and not equal to one. In this case, the SAC value is exactly 1 but the objective in this application is not really achieved. Consequently, CSF of the i-th DOF is also employed herein with expression as

$$\mathrm{CSF}^i = \frac{2|\boldsymbol{u}^* \cdot \boldsymbol{v}|}{|\boldsymbol{u}^* \cdot \boldsymbol{u}| + |\boldsymbol{v}^* \cdot \boldsymbol{v}|} \tag{19}$$

An integrated application of SAC and CSF allows that the comparison between two FRFs is not only the degree of correlation but essentially the error between them. Note that the above definition of SAC and CSF are based on a single DOF of FRF, i.e. each row of the $n \times N$ matrix. A complete comparison between two sets of FRFs with n DOFs is defined as

$$f(\mathbf{M}, \mathbf{K}, \mathbf{C}) = \frac{1}{n}\sum_i^n \left(\frac{\mathrm{SAC}^i + \mathrm{CSF}^i}{2}\right) \tag{20}$$

where the superscript i is the index of DOF. A comprehensive comparison between two sets of n-DOF FRFs with both resonant and auto-resonant frequencies is provided by the above objective function, whose feasibility is conformed in the following example sections.

3 Optimization tools

After the uncertainty boundary and objective function are defined, the calibration procedure can be essentially described as an optimization problem:

$$\begin{gathered}\text{Starting from } (\mathbf{M}_p, \mathbf{K}_p, \mathbf{C}_p),\\ \text{find } (\widetilde{\mathbf{M}}, \widetilde{\mathbf{K}}, \widetilde{\mathbf{C}}), \text{ minimizing } f\left(\widetilde{\mathbf{M}}, \widetilde{\mathbf{K}}, \widetilde{\mathbf{C}}\right),\\ \text{while } (\widetilde{\mathbf{M}}, \widetilde{\mathbf{K}}, \widetilde{\mathbf{C}}) \text{ fall within the uncertainty boundary,}\end{gathered} \tag{21}$$

where the subscript p denotes the preliminary matrices obtained after the deterministic identification procedure (refer to the unsteady matrices in Fig. 1). This optimization problem contains the following difficulties, which make an explicit solution almost impossible.

1) A large number of variables to be optimized. A n-DOF structure, whose system matrices are symmetric, has $3n(n+1)/2$ parameters. For example, a simple 4-DOF system leads to 30 optimizing parameters.
2) A complex objective function. The relationship between the objective function and the parameters is implicit, nonlinear, and complex. The gradient information is difficult to be determined.

To solve these difficulties, the Genetic Algorithm (GA) and various constraint minimization methods are proposed as the optimization tool, as shown in Fig. 1. The GA is a population-based searching algorithm inspired by natural evolution functions such as selection, crossover, and mutation [25]. The GA is popular in academic and industrial fields because of its simple principle, extensive application range, and feasibility of solving large-scale, highly nonlinear and complex problems. It is capable of finding the global solution in the overall search space, however, the result of GA can be unsteady and the calculation cost is expensive for complex applications. As a supplement, the classical constrained minimization methods, e.g. simplex algorithm and interior point method [26], are proposed following the GA to obtain a consistent solution with improved precision.

Note that the objective of this section is not to develop a new optimization algorithm but to appropriately configure the optimization problem, such as the boundary and objective function, and then to propose suitable optimization tools to solve the problem. Depending on the complexity of each specific application, the selection of the optimization tools can be changed. For example, in a simple case with small DOF and reduced uncertainty, only the classical constrained minimization method is probably enough to obtain a solution with equivalent precision. Consequently, it is the reader's choice to select other computational intelligence techniques such as particle swarm [27] or simulated annealing [28], based on the consideration of precision and calculation cost. Not actually being the main focus of this work, the comparison of different optimization tools' performance is omitted for clarity.

4 Validation metric

As shown in Fig. 1, m sets of optimized matrices, $\widetilde{\mathbf{M}}_i, \widetilde{\mathbf{K}}_i, \widetilde{\mathbf{C}}_i$ $(i = 1, \ldots, m)$, are obtained after the calibration procedure. Different from the unsteady matrices after the properness enforcement procedure, the final optimized matrices are expected to represent the property of the same structure. The discrepancy among different sets should be limited (demonstrated in the following Sections III and IV), and hence they are termed as steady matrices. The so-called mean coefficient of variation (MCV) is proposed as the validation metric to quantitatively measure the degree of steadiness of these optimized matrices.

$$\mathrm{MCV} = \frac{1}{n^2}\sum_{i=1}^{n}\sum_{j=1}^{n}\delta_{ij}^{ele}, \tag{22}$$

where n is the number of DOFs (i.e. the dimension of the matrix); δ_{ij}^{ele} is the coefficient of variation of each element in the matrix, which is defined by the ratio of the standard deviation σ to the absolute value of mean $|\mu|$, i.e. $\delta^{ele} = \sigma/|\mu|$.

As the final result of this approach, the statistical features (e.g. the mean and standard deviation) of the matrices are estimated from the steady matrix sample. The statistical features can be served as the guideline of the matrices' further application with desirable robustness corresponding to the experimental uncertainty.

III. Numerical example

A. Description of the basic procedure

In this section, the overall identification and calibration approach is demonstrated by a simulated test-case, which starts from the pre-defined 5-DOF system matrices:

$$\underbrace{\begin{bmatrix} 2.14 & -1.79 & 0.86 & -2.50 & -3.34 \\ -1.79 & 1.80 & -0.60 & 1.93 & 2.58 \\ 0.86 & -0.60 & 0.87 & -1.74 & -2.26 \\ -2.50 & 1.93 & -1.74 & 5.59 & 7.06 \\ -3.34 & 2.58 & -2.26 & 7.06 & 9.29 \end{bmatrix}}_{\mathbf{M}} \{\ddot{\mathbf{x}}\} + \underbrace{\begin{bmatrix} 27.2 & -44.3 & -1.72 & -20.4 & -39.8 \\ -44.3 & 60.9 & -2.19 & 13.3 & 35.7 \\ -1.72 & -2.19 & 1.07 & -8.16 & -6.07 \\ -20.4 & 13.3 & -8.16 & 87.5 & 109 \\ -39.8 & 35.7 & -6.07 & 109 & 124 \end{bmatrix}}_{\mathbf{C}} \{\dot{\mathbf{x}}\}$$
$$+ \underbrace{\begin{bmatrix} 0.53\times10^{6} & -0.43\times10^{6} & 0.42\times10^{6} & -1.07\times10^{6} & -1.27\times10^{6} \\ -0.43\times10^{6} & 0.51\times10^{6} & -0.19\times10^{6} & 0.71\times10^{6} & 0.85\times10^{6} \\ 0.42\times10^{6} & -0.19\times10^{6} & 0.58\times10^{6} & -1.08\times10^{6} & -1.28\times10^{6} \\ -1.07\times10^{6} & 0.71\times10^{6} & -1.08\times10^{6} & 2.49\times10^{6} & 2.89\times10^{6} \\ -1.27\times10^{6} & 0.85\times10^{6} & -1.28\times10^{6} & 3.40\times10^{6} & 3.40\times10^{6} \end{bmatrix}}_{\mathbf{K}} \{\mathbf{x}\} = 0. \quad (23)$$

Although it is a numerical example, the pre-defined system matrices are representative of a physical system, since they are identified from the experimental setup presented in Section IV. As shown in Fig. 2, the example follows the key steps:

1. Calculation of the original data: The original FRFs and modes are theoretically calculated based on the pre-defined matrices. The original data (FRFs, natural frequencies, and matrices) will be served as the reference in the following comparison.

2. Simulation of the experimental uncertainty: Ten percent uniform random noise is added to the original eigenvectors and eigenvalues. In practical experiments, the identified eigenvalues are generally more precise than the identified eigenvectors [17]. However, in this simulated example, the noise level of the eigenvalues is proposed as high as that of the eigenvectors. This special treatment is intended to demonstrate the approach's performance on not only damping but also mass and stiffness terms. This step is repeated five times, generating five sets of noised modes (designated as Case #*i*, *i*=1, 2, …, 5). As shown in Fig. 2, the deterministic identification procedure is separately performed in each case.

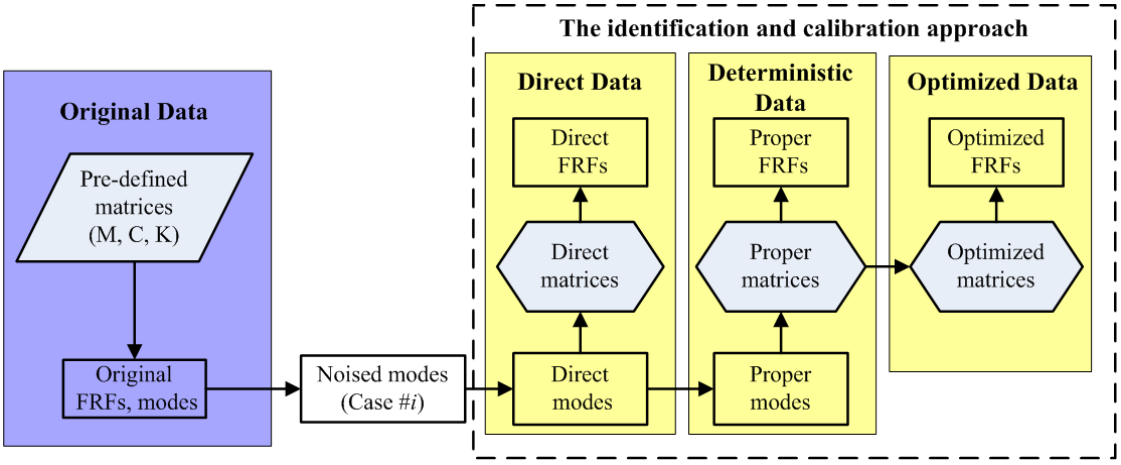

Fig. 2: Key procedures of the numerical example in the *i*th case (*i*=1, 2, …, 5)

3. Identification of each noised case: As shown in Fig. 2, there are three categories of output data, depending on which techniques are performed on the data.

- "Direct" data: no calibration technique is performed on the modes before they are utilized to construct the matrices and calculated the FRF. This is why the data is designated after "Direct".
- "Deterministic" data: the properness enforcement method is performed on the modes, and afterwards the proper matrices and FRF are calculated. There is no uncertainty information processed till now, hence the data is designated after "Deterministic".
- "Optimized" data: the integrated optimization procedure is additionally performed on the proper matrices, with the purpose of minimizing the discrepancy between the optimized FRF and the benchmark FRF.

The direct, proper, and optimized data is compared to assess whether the finally obtained matrices can represent the original system behavior.

4. Cross comparison among different cases: this step focuses on the uncertainty of different experiments. The five sets of optimized matrices will be compared to assess whether they can converge to the original data. This step is specially designed to demonstrate the overall approach's ability for robust damping identification with regard to the uncertainties in experiments.

B. Assessment of the single noised Case #1

Considering the direct data in Fig. 2, the complex modes are directly utilized in the inverse procedure to construct the direct matrices, which are undoubtedly different from the original pre-defined matrices because of the random noise. Alternatively, the direct modes are calibrated by the properness enforcement method, after which the deterministic data (matrices and FRF) is calculated as a comparison with the direct data. In addition to the deterministic procedure, the proper matrices are furthermore optimized using the probabilistic calibration procedure.

Based on these three sets (direct, deterministic, and optimized) of matrices, the natural frequencies are calculated and compared with the original data as listed in Table 1. As there is 10% random noise in the eigenvalues, the direct natural frequencies exhibit considerable error compared with the original ones. It is interesting to observe that the errors of the deterministic frequencies are not clearly reduced by the properness enforcement method. This can be easily explained from Eqs. (14-15) where the properness enforcement method can only calibrate the eigenvectors, but not the eigenvalues. Nevertheless, the following calibration procedure is capable of calibrating the mass and stiffness matrices, making the error of the optimized frequencies extremely low.

Table 1: Natural frequencies (% percent errors in parentheses compared with the original data)

	Original	Direct	Deterministic	Optimized
f_1 (Hz)	20.90	21.68 (3.62)	21.65 (3.48)	20.90 (0.12)
f_2 (Hz)	42.25	40.57 (-4.13)	40.57 (-4.15)	42.25 (0.004)
f_3 (Hz)	70.44	68.24 (-3.23)	68.29 (-3.16)	70.37 (-0.10)
f_4 (Hz)	105.41	112.62 (6.41)	110.48 (4.59)	105.45 (0.04)
f_5 (Hz)	146.95	159.82 (8.05)	150.73 (2.51)	146.97 (0.01)
Absolute mean error		5.09%	3.58%	0.04%

The natural frequencies are calculated using the stiffness and mass matrices, implying that the errors in Table 1 cannot demonstrate the precision of the damping matrix. Consequently, the FRFs are utilized to compare with the original FRF with the purpose of damping assessment. The direct, deterministic, and optimized FRFs are calculated using the corresponding matrices and a unit force $\mathbf{F}=[1, 0, 0, 0, 0]^T$. The original, direct, deterministic and optimized FRFs are compared in Fig. 3.

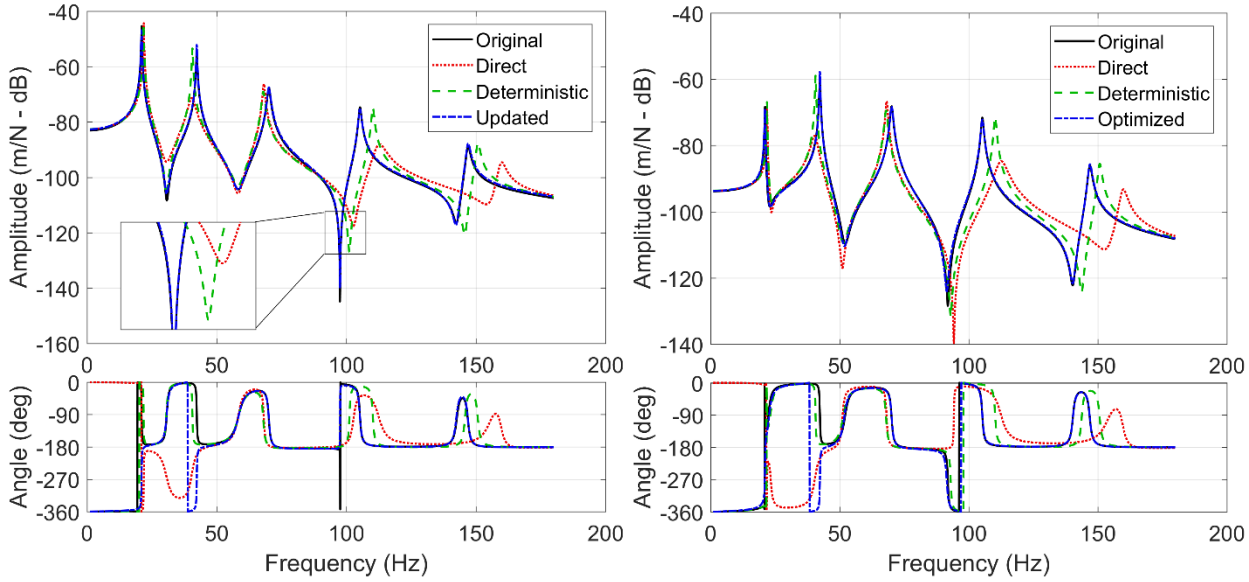

(a) the 1st DOF

(b) the 2nd DOF

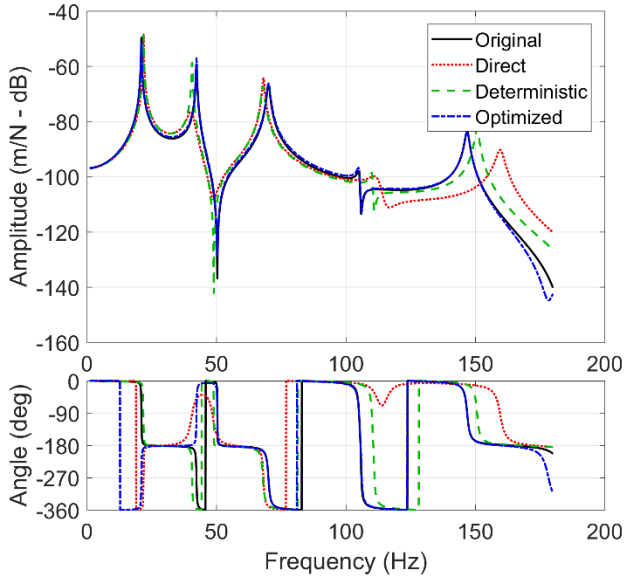

(c) the 3rd DOF

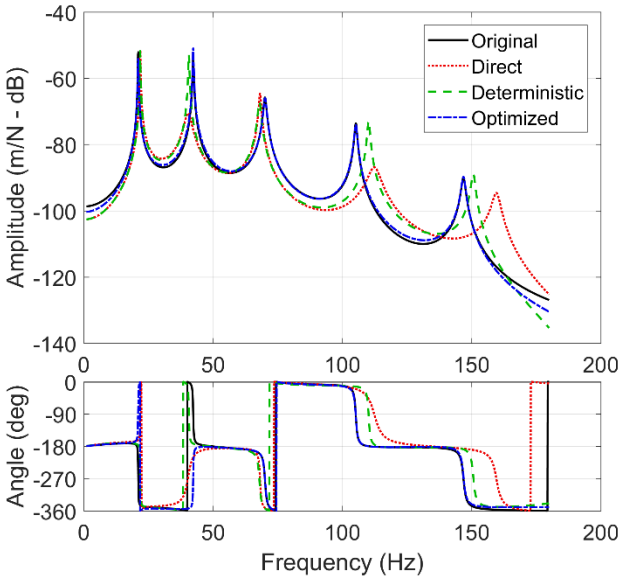

(d) the 4th DOF

Fig. 3: The original, direct, deterministic and optimized FRFs of Case #1

The first four DOFs of the system are presented in Fig. 3, where a similar tendency is observed among the subfigures. The direct FRFs clearly fail to represent the original FRFs at both resonant and anti-resonant frequencies. This is naturally caused by the random noise in the direct modes, which is not suitably managed by any calibration technique. After the properness enforcement in the deterministic identification, the deterministic FRFs are improved, however, only at the maximum points of the amplitudes. Other key quantities such as minimum points of the amplitudes, the resonant and anti-resonant frequencies,

which are sensitive to the damping features, are not improved. As a comparison, the finally optimized FRFs perfectly coincide with the original FRFs, showing that the calibration procedure is capable of obtaining the system matrices, which can represent the similar system behaviors as the original ones.

A more obvious assessment of the matrix, in this simulated case, is performed by comparing the identified matrices with the pre-defined matrices. The comparison of the matrices is performed as

$$error = \frac{\|\mathbf{A}_{id} - \mathbf{A}_{pre}\|}{\|\mathbf{A}_{pre}\|} \times 100\% \tag{24}$$

where $\mathbf{A}_{id}$ is the identified matrix (mass, stiffness, or damping); $\mathbf{A}_{pre}$ is the pre-defined matrix; $\|\blacksquare\|$ denotes the Euclidian norm of a matrix.

The relative errors of the direct, deterministic, and optimized matrices, compared with the pre-defined matrices, are listed in Table 2. Considering the row of stiffness, the deterministic errors are clearly reduced from the direct errors, while the error of the optimized stiffness is not obviously changed compared with the deterministic error. As for the row of mass, the direct error is already quite small in this specific case, thus the calibration effect in the deterministic and optimized data is not obvious. It makes more sense to check the last row of Table 2 where the damping errors are quite high for both direct and deterministic data, while for the optimized data the damping error is significantly reduced by the calibration procedure. This clearly demonstrates that the overall approach is capable of identifying and calibrating not only the mass and stiffness, but also the damping.

Table 2: The matrice error compared with the pre-defined matrices in Case #1

	Direct	Deterministic	Optimized
Stiffness: **K**	23.4%	6.99%	5.79%
Mass: **M**	6.81%	7.56%	9.53%
Damping: **C**	67.2%	87.8%	12.0%

C. Cross validation of different cases

This subsection focuses on the uncertainty in multiple experiments, which are simulated by the random noise added to the eigenvalues and eigenvectors in Cases #1-#5. The idea is, if the finally obtained matrices in different cases simultaneously converge to the pre-defined one, the ability of the overall identification to handle the experimental uncertainty would be confirmed.

The stability of the results in different cases is firstly checked by the FRFs as illustrated in Fig. 4, where the five deterministic FRFs from different cases are clearly discrepant. As a comparison, the five optimized FRFs (blue) are completely coincident with the original FRF (black).

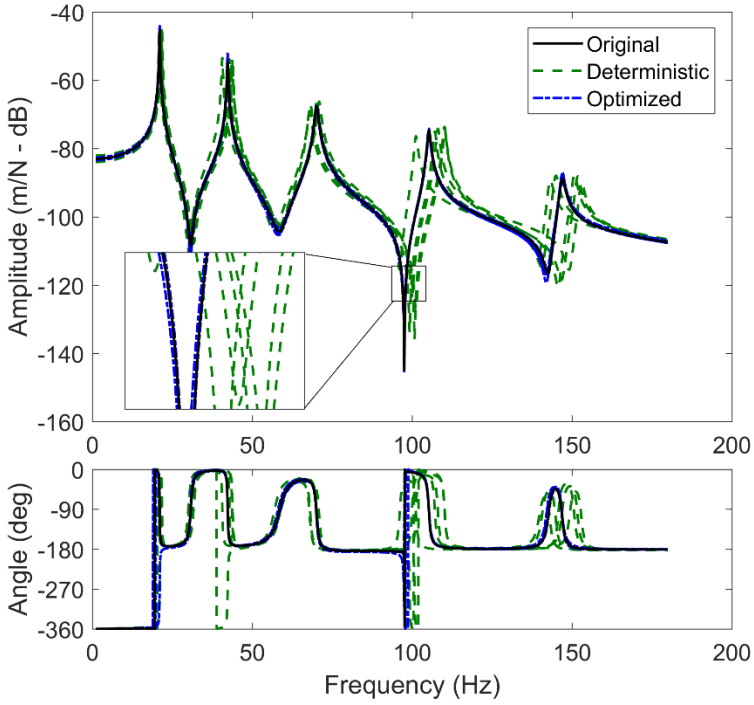

Fig. 4: The original, proper, and optimized FRFs of Cases #1-#5 on the 1st DOF

As the final objective is the system matrices, it makes more sense to check if the optimized matrices among different cases are steady. The validation metrics are illustrated in Fig. 5, where the MCV of mass, damping, and stiffness matrices are compared. In the direct data, it is clearly shown that the MCV of damping is significantly higher than those of mass and stiffness, demonstrating the damping term is more sensitive to the noise than the mass and stiffness terms. In the deterministic data, the MCV of damping does not exhibit clear reduction compared with the one in the direct data, implying the deterministic procedure is insufficient to cope uncertainty in different cases. As a comparison, in the optimized data, the MCV of damping is significantly reduced by the calibration procedure, after which more steady damping matrices are available. As the final result, the mean and standard deviation of the optimized mass, stiffness, and damping matrices are given in Appendix.

In this cross validation, however, it is not surprising to find the optimized results of Cases #1-5 are steady, because all optimization procedures are using the same original FRF as benchmark. Nevertheless, the above results demonstrate that the probabilistic definition of uncertainty boundary and the integrated application of SAC and CSF to define the objective function in the calibration procedure are feasible. More interesting result is presented in the following experimental example, where different experimental FRFs are employed as benchmarks in different calibration procedures.

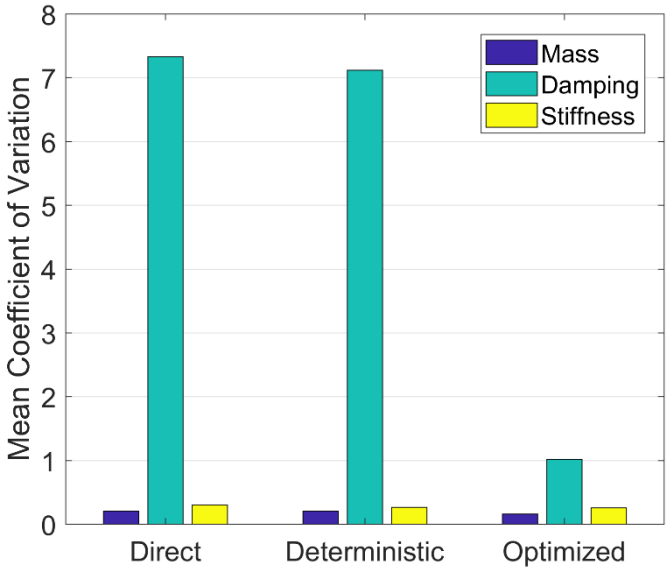

Fig. 5: Mean coefficient of variation of the matrices in the direct, deterministic, and optimized data

IV. Experimental example

A. Experiment setup

An aluminum beam with periodic thickness is proposed in this example, as shown in Fig. 6. Five accelerometers are used to measure the response of the beam. The 1st and 5th measure points are shown in Fig. 6(b) while the other 3 measure points, which also distribute along the central axis of the beam, are omitted in the figure. The distances from the right endpoint of the beam to these five measure points are respectively 10 mm, 134 mm, 433 mm, 885 mm, and 1038.5 mm.

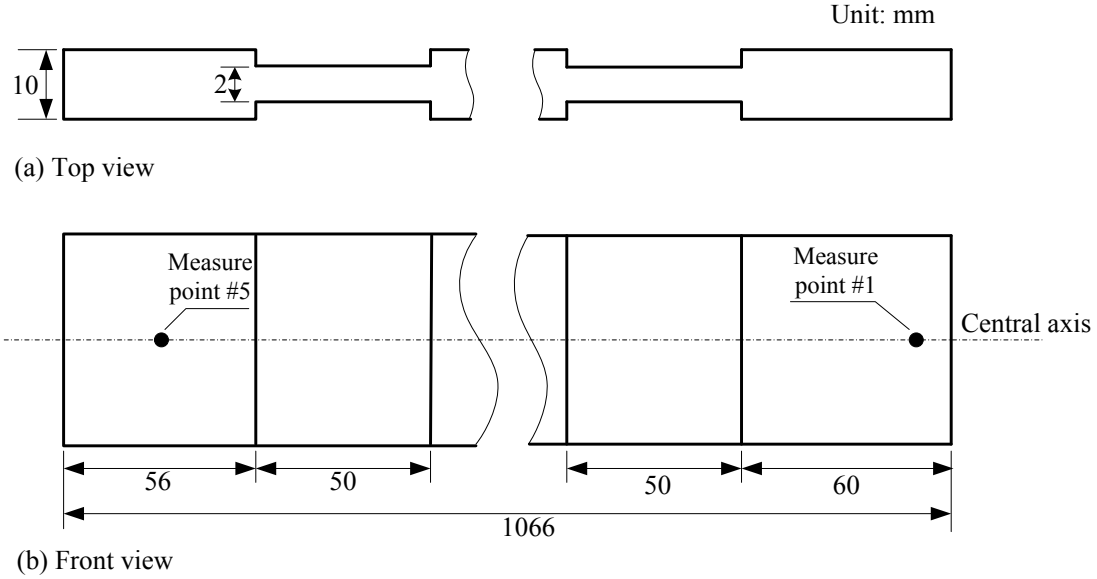

Fig. 6: The geometry detail of the periodic beam (dimensions in mm)

The experimental setup is illustrated in Fig. 7 where free-free conditions are used, and six resin badges (40×50 mm^2) are stuck on the beam to improve the damping effect. Five experiments are executed on the same beam but with different excitations. Corresponding to the excitation position, the experiments are designated as Case #1-#5. In Case #1, a magnetic exciter (Fig. 7b) is utilized to excite the beam at the 1st measure point. In the following four cases, the beam is excited by an impact hammer (Fig. 7c) respectively at the 2nd-5th measure points. Compared with fixed conditions, the free-free conditions proposed herein are more sensitive to the environment noise. Moreover, among different cases, it is impossible to perfectly control the force amplitude, direction, and position of the hammer impact. This multiple experiments setup is specially designed to involve most hard-to-control random effects and uncertainties in practical vibration experiments.

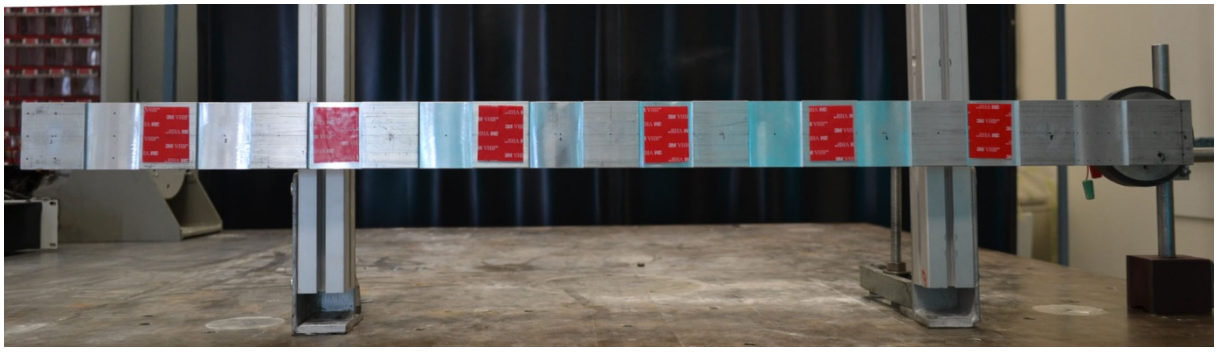

(a) View of the suspended beam

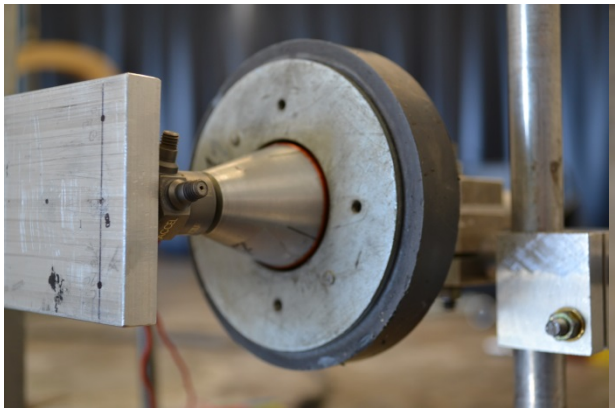

(b) View of the magnetic exciter

(c) View of the impact hammer

Fig. 7: Setup of the experiment

Note that, in practical operation, it is more common to use the hammer to excite all measurement points. Then multiple groups of FRFs with different reference points are combined as a complete set of FRFs, which is further utilized for identification. However, in this example, the special treatment to separate each group of FRFs as a single experiment is intended for a full investigation of uncertainty relative to the force amplitude, direction, and position of the hammer impact. Another expectation of this special treatment is to check whether the finally obtained matrices can converge to a steady result even if the benchmark FRFs are different.

B. Assessment of the single experimental case

This example focuses on the frequency range 15-160Hz where the first five modes of the beam are identified. The assessment process is similar as what is shown in Fig. 2, however, without the pre-defined matrices and directly stating from the experimental FRFs. The overall approach's ability on damping identification and calibration is firstly demonstrated in two single cases. Case #1 (with magnetic exciter) and Case #5 (with hammer) are respectively assessed as follows, while the assessment of the remaining three cases is omitted for clarity. The cross comparison and validation among all the five cases is presented in the Section IV.C.

1 Case #1: Vibration excitation (magnetic exciter)

The natural frequencies are firstly compared in Table 3. The high error of the direct frequencies clearly shows that the direct identified matrices are far from the physical values. The absolute mean error of the deterministic frequencies is significantly reduced to an extremely low level, which confirms the properness enforcement method's feasibility on mass and stiffness identification. Note that the result herein is different from that in the simulated example (Table 1) where the error of deterministic data was not perfectly reduced. Explanation for this phenomenon is, in this example, the identified eigenvalues contain little error while most error is involved in the eigenvectors, which can be appropriately calibrated by the deterministic identification procedure. Nevertheless, comparison of natural frequencies can only reflect the precision of mass and stiffness. Consequently, the FRFs are compared to assess the identified damping term.

The experimental, direct, deterministic, and optimized FRFs in Case #1 are presented in Fig. 8. The direct FRFs clearly fail to represent the experimental FRFs at neither the resonant frequencies nor the anti-resonant frequencies. More attention should be paid on the difference between the deterministic and optimized FRFs, especially for the amplitudes at the resonant and anti-resonant frequencies. The amplitudes of deterministic FRFs at both resonant and anti-resonant frequencies are different from those of the experimental FRFs. As a comparison, the optimized FRFs (in blue) perfectly coincide with the experimental benchmark (in black).

Table 3: Comparison of the natural frequencies of Case #1 (% percent error in parentheses)

Modes No.	Experimental	Direct	Deterministic	Optimized
f_1 (Hz)	21.01	20.91 (-0.48)	20.87 (-0.67)	20.79 (-1.03)
f_2 (Hz)	42.36	42.64 (0.66)	42.28 (-0.19)	42.18 (-0.41)
f_3 (Hz)	70.07	70.85 (1.11)	70.08 (0.01)	70.15 (0.12)
f_4 (Hz)	105.2	107.8 (2.47)	105.3 (0.10)	105.7 (0.48)
f_5 (Hz)	146.9	852.1 (480)	148.0 (0.75)	148.3 (0.98)
Absolute mean error		97.0%	0.34%	0.60%

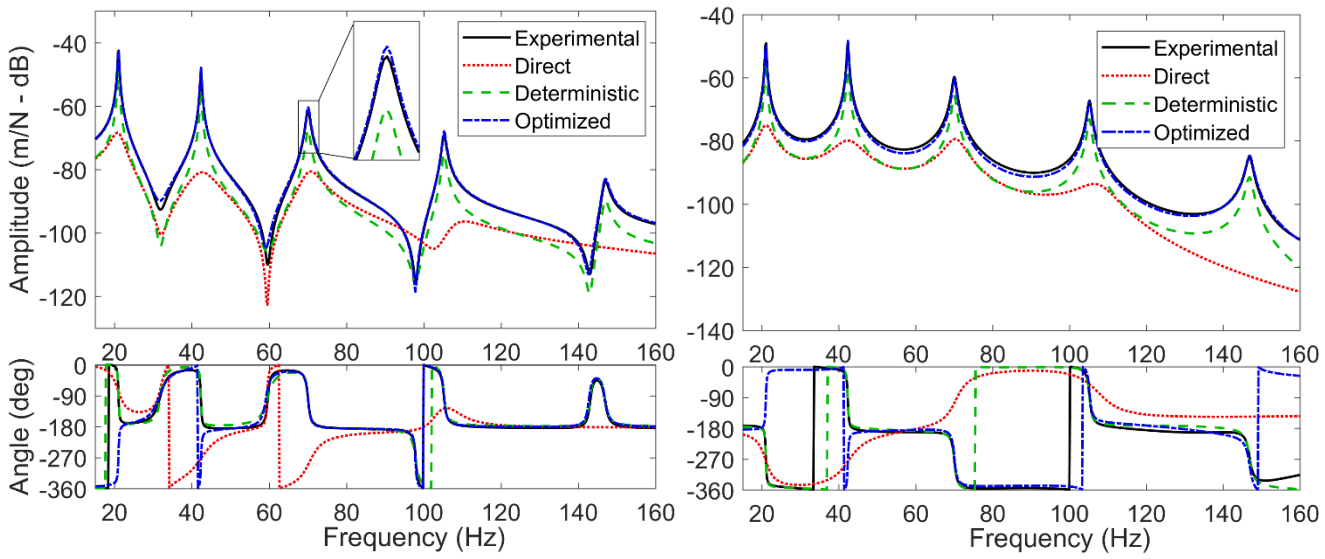

(a) The 1st DOF (b) The 4th DOF

Fig. 8: The comparison among the FRFs of Case #1

2 Case #5: Impact excitation (hammer)

Another experimental case with the hammer impacted on the 5th measure point is presented in this subsection. Comparison of the natural frequencies and the FRFs are respectively given in Because the position of the excitation is changed between Case #1 and Case #5, the FRFs in Fig. 9 are completely different from those shown in Fig. 8. However, the comparison of the FRFs has similar conclusions as the optimized FRFs fit with the experimental FRFs better than the deterministic FRFs at the anti-resonant frequencies, for example, nearby 100Hz in Fig. 9(b).

Table 4 and Fig. 9, where the similar effect as Case #1 is exhibited.

The experimental frequencies in Because the position of the excitation is changed between Case #1 and Case #5, the FRFs in Fig. 9 are completely different from those shown in Fig. 8. However, the comparison of the FRFs has similar conclusions as the optimized FRFs fit with the experimental FRFs better than the deterministic FRFs at the anti-resonant frequencies, for example, nearby 100Hz in Fig. 9(b).

Table 4 are slightly different from those shown in Table 3. This is caused by the uncertainty in different experiments which will be further investigated in the following section. The direct natural frequencies are unphysical due to incorrect mass and stiffness matrices. The deterministic and optimized frequencies have similar performances as those obtained from Case #1, where the errors of the deterministic and optimized frequencies are both small.

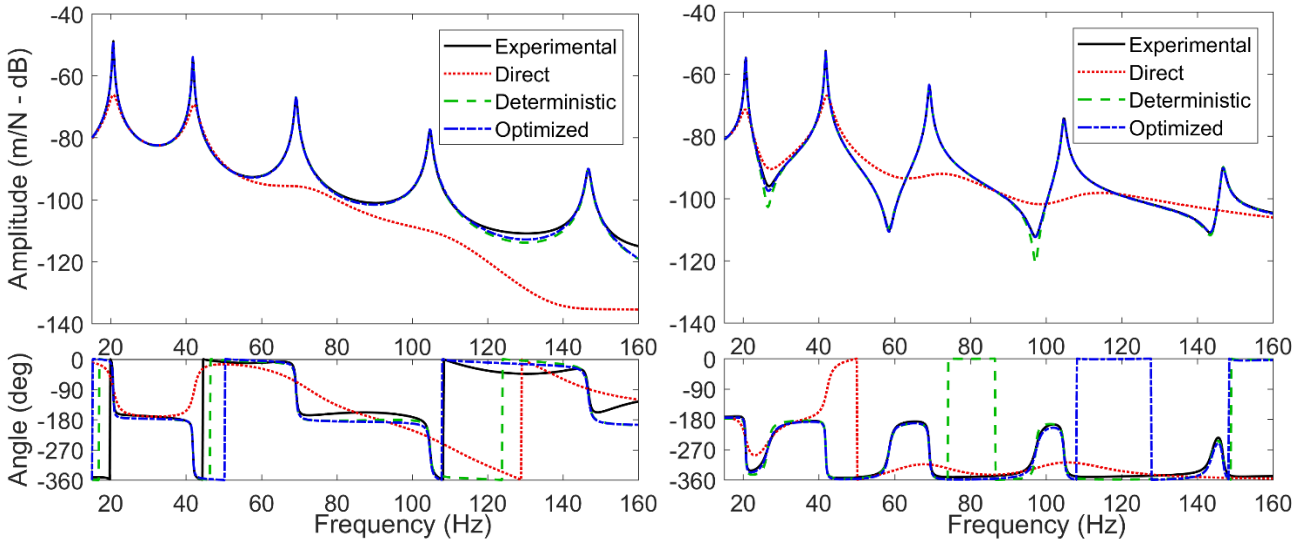

(a) The 1st DOF (b) The 4th DOF

Fig. 9: The comparison among the FRFs for Case #5

Because the position of the excitation is changed between Case #1 and Case #5, the FRFs in Fig. 9 are completely different from those shown in Fig. 8. However, the comparison of the FRFs has similar conclusions as the optimized FRFs fit with the experimental FRFs better than the deterministic FRFs at the anti-resonant frequencies, for example, nearby 100Hz in Fig. 9(b).

Table 4: Comparison of the natural frequencies of Case #5 (% percent error in parentheses)

Modes No.	Experimental	Direct	Deterministic	Optimized
f_1 (Hz)	20.64	0 (-100)	20.53 (-0.57)	20.51 (-0.63)
f_2 (Hz)	41.82	20.42 (-56.2)	41.81 (-0.02)	41.85 (0.07)
f_3 (Hz)	69.20	42.17 (-39.1)	69.29 (0.14)	69.25 (0.08)
f_4 (Hz)	104.8	72.40 (-30.9)	104.8 (0.09)	104.8 (0.06)
f_5 (Hz)	146.8	114.0 (-22.3)	147.3 (0.36)	147.4 (0.43)
Absolute mean error		48.7%	0.24%	0.25%

C. Cross validation of the five experimental cases

In this cross comparison among Cases #1-#5, more attention is paid on the influence of the experimental uncertainty on the damping terms. As mentioned in the previous section, the FRFs in different cases are different from each other. Hence the cross comparison of the FRFs as performed in the simulated example (Fig. 4) is no longer meaningful in this experimental example. However, the final objective of this work is not the FRFs but the system matrices. Even the type and position of the excitation is different in each case, the finally obtained mass, stiffness, and damping matrices of the beam are expected to be steady among Cases #1-#5.

Similar as the simulated example, the MCV is proposed as validation metric to quantify the dispersion of different matrices. The comparison of the MCVs is respectively performed in different types of data (i.e. direct, deterministic, and optimized data) as illustrated in Fig. 10. In the direct data, the matrix MCVs, especially for the damping matrix, are quite large, implying the

damping matrices are quite sensitive to the experimental uncertainty. The MCV of the stiffness matrices is also big, which explains the incorrect natural frequencies in the previous subsection (recall Table 3 and Because the position of the excitation is changed between Case #1 and Case #5, the FRFs in Fig. 9 are completely different from those shown in Fig. 8. However, the comparison of the FRFs has similar conclusions as the optimized FRFs fit with the experimental FRFs better than the deterministic FRFs at the anti-resonant frequencies, for example, nearby 100Hz in Fig. 9(b).

Table 4).

A more interesting phenomenon is revealed by the MCVs of the deterministic matrices. First, the MCV of the stiffness matrix is clearly reduced, implying the feasibility of the properness enforcement method on stiffness identification. However, the MCV of the damping matrix is not reduced but significantly amplified. This means the damping matrices after the deterministic identification are quite different in each case. In practical application, if the identification process stops at the deterministic data, the engineer would only arbitrarily adopt a result from a single experimental case, which could lead to a significant error in the following application.

The probabilistic calibration procedure is consequently critical to solve the above problem. As shown in Fig. 10, the MCVs of the optimized mass, damping and stiffness matrices are all minimized. The damping MCV is slightly larger than the mass and stiffness MCVs, however, this is an acceptable result as the damping term is naturally more sensitive than the mass and stiffness terms. Note that, during the optimization process, different FRFs are taken as benchmarks in different cases. Even though the benchmarks are different, the finally obtained matrices can still converge to a similar value, which clearly conforms the overall approach's ability on robust damping identification with regard to the experimental uncertainty.

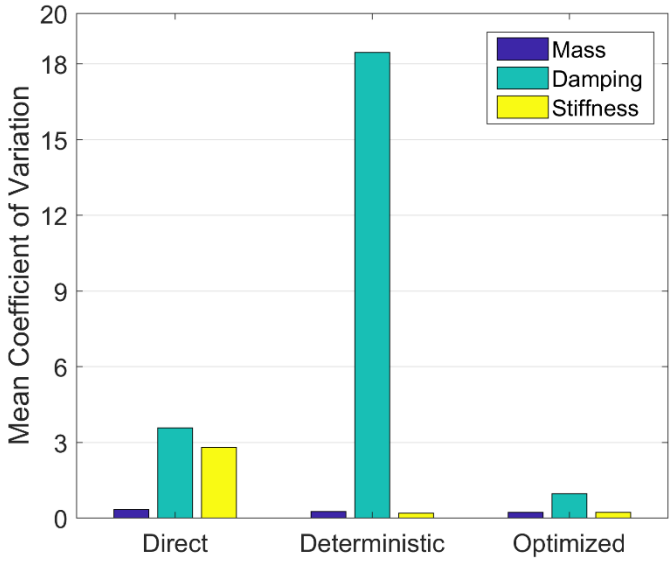

Fig. 10: Mean coefficient of variation of the matrices among the five experimental cases

V. Conclusions and perspectives

An overall identification and calibration approach for mass, stiffness, and especially damping matrices is proposed in this paper. Emphases are put on the probabilistic calibration procedure, where the uncertainty information from experiments is appropriately disposed.

As the first part of this approach, the deterministic identification procedure utilizes the properness enforcement technique to construct the system matrices. Two open questions of this widely used technique are revealed: 1) This technique can only calibrate the eigenvectors, but not the eigenvalues. In the presence of noise/error in eigenvalues, precisions of the identified natural frequencies, mass and stiffness matrices cannot be guaranteed. 2) Even if the mass and stiffness matrices are correctly identified, the experimental uncertainty can significantly influence the damping matrix.

Considering the above problems, a probabilistic calibration procedure is proposed. The uncertainty boundary is defined with a confidence degree based on Gaussian distribution. This treatment is objective and practical as a limited number of experiments is sufficient in real operation. The integrated application of SAC and CSF in the objective function provides a comprehensive comparison between two sets of FRFs. Feasibility of the probabilistic calibration is demonstrated in the examples where a validations metrics of matrix steadiness is also examined. The experimental example presents a challenging mission by utilizing both magnetic exciter and hammer excited on different positions of the beam, which naturally involves much more experimental uncertainties in practical operations. Nevertheless, the finally identified damping matrices exhibit satisfied robustness.

A limitation of this approach is that the applicative problem scale is not large. A large number of modes (i.e. system DOFs) requires a significant increase of the optimal parameters, which probably leads to failure of the optimization procedure. A more refined optimization procedure is consequently a meaningful extension of this work. It should be note that the objective of this overall approach is to reconstruct matrices for an equivalent system of the physical structure, which can represent the same behaviors as the experimentally measured ones, within a certain frequency range defined by the measured natural frequencies. Hence the feasibility of the obtained matrices is limited within the active frequency range. Nevertheless, the current approach is feasible in practical application, because the realistic requirement always focuses on a specific frequency range with a finite number of modes rather than all modes in an infinite range at the same time. With small calculation cost, the finally obtained system matrices can be served as a necessary supplement of the popular finite element method, especially in fields such as system health monitoring and vibration active controlling. Another perspective is proposed based on the fact that the current work is limited on viscous damping. Further assessment and development of this approach on various damping models will be the next step work.

In real-life engineering, the exact and unique answer of damping identification is always hidden behind the mist of uncertainty. By providing a set of steady solutions with the estimated mean and standard deviation, the proposed approach demonstrates its ability to pursuit the numerical value which is robust to the physical truth, in the presence of inherent experimental uncertainties.

Acknowledgments

The Authors gratefully acknowledge Romeo Lecomte for their assistance on the measurements utilized in the experimental example. This work was co-financed by the French National Research Agency under grant number ANR-12-JS09-008-COVIA. It has been performed in cooperation with the Labex ACTION program (ANR-11-LABX-0001-01). The first author is supported by the Alexander von Humboldt Foundation, which is greatly acknowledged. The authors are particularly grateful to the anonymous reviewers who considerably helped to improve the manuscript.

Appendix

In the numerical example (Section III), the statistical features of the mass, stiffness, and damping matrices are respectively listed as follows:

1. The mean of each element in damping matrix:

$$\begin{bmatrix} 28.6 & -43.4 & -1.82 & -19.0 & -36.4 \\ -43.4 & 58.5 & -1.00 & 7.42 & 26.8 \\ -1.82 & -1.00 & 0.80 & -7.26 & -3.79 \\ -19.0 & 7.42 & -7.26 & 85.0 & 100 \\ -36.4 & 26.8 & -3.79 & 100 & 107 \end{bmatrix}. \tag{A.1}$$

The standard deviation of each element in the damping matrix:

$$\begin{bmatrix} 4.94 & 2.46 & 2.37 & 6.89 & 8.64 \\ 2.46 & 4.00 & 2.74 & 3.66 & 5.14 \\ 2.37 & 2.74 & 1.23 & 11.9 & 15.0 \\ 6.89 & 3.66 & 11.9 & 31.1 & 41.6 \\ 8.64 & 5.14 & 15.0 & 41.6 & 55.9 \end{bmatrix}. \tag{A.2}$$

2. The mean of each element in the mass matrix:

$$\begin{bmatrix} 2.16 & -1.77 & 0.67 & -2.10 & -2.80 \\ -1.77 & 1.77 & -0.43 & 1.55 & 2.07 \\ 0.67 & -0.43 & 0.69 & -1.26 & -1.60 \\ -2.10 & 1.55 & -1.26 & 4.37 & 5.37 \\ -2.80 & 2.07 & -1.60 & 5.37 & 6.97 \end{bmatrix}. \tag{A.3}$$

The standard deviation of each element in the mass matrix:

$$\begin{bmatrix} 0.41 & 0.28 & 0.10 & 0.32 & 0.55 \\ 0.28 & 0.25 & 0.07 & 0.30 & 0.39 \\ 0.10 & 0.07 & 0.10 & 0.18 & 0.26 \\ 0.32 & 0.30 & 0.18 & 0.46 & 0.62 \\ 0.55 & 0.39 & 0.26 & 0.62 & 0.98 \end{bmatrix}. \tag{A.4}$$

3. The mean of each element in stiffness matrix:

$$\begin{bmatrix} 0.53 & -0.41 & 0.35 & -0.93 & -1.07 \\ -0.41 & 0.50 & -0.12 & 0.58 & 0.67 \\ 0.35 & -0.12 & 0.48 & -0.86 & -0.99 \\ -0.93 & 0.58 & -0.86 & 2.00 & 2.25 \\ -1.07 & 0.67 & -0.99 & 2.25 & 2.58 \end{bmatrix} \times 10^6. \tag{A.5}$$

The standard deviation of each element in the stiffness matrix:

$$\begin{bmatrix} 1.92 & 1.18 & 0.94 & 2.08 & 2.91 \\ 1.18 & 0.82 & 0.68 & 1.60 & 1.95 \\ 0.94 & 0.68 & 0.76 & 1.33 & 1.86 \\ 2.08 & 1.60 & 1.33 & 2.70 & 3.69 \\ 2.91 & 1.95 & 1.86 & 3.69 & 5.25 \end{bmatrix} \times 10^5. \quad \text{(A.6)}$$

References

[1] Adhikari, S., and Woodhouse, J., "Identification of Damping: Part 1, Viscous Damping," Journal of Sound and Vibration, Vol. 243, No. 1, May 2001, pp. 43–61.
doi: 10.1006/jsvi.2000.3391.

[2] Rayleigh, L., Theory of Sound (two volumes), New York: Dover Publications, 1945 re-issued, second edition: 1877.

[3] Li, L., and Hu, Y., "State-Space Method for Viscoelastic Systems Involving General Damping Model," AIAA Journal, Vol. 54, No. 10, 2016, pp. 1–6.
doi: 10.2514/1.J054180.

[4] Ding, Z., Li, L., and Hu, Y., "A modified precise integration method for transient dynamic analysis in structural systems with multiple damping models," Mechanical Systems and Signal Processing, Vol. 98, 2018, pp. 613–633.
doi: 10.1016/j.ymssp.2017.05.018.

[5] Crawley, E. F., and Mohrt, D. G., "Experimental Measurements of Material Damping in Free Fall with Tunable Excitation," AIAA Journal, Vol. 23, No. January 1985, Jan. 1984, pp. 125–131.
doi: 10.2514/3.8880.

[6] Baburaj, V., and Matsuzaki, Y., "A Study on the Material Damping of Thin Angle-Ply Laminated Plates," Journal of Sound and Vibration, Vol. 172, No. 3, May 1994, pp. 415–419.
doi: 10.1006/jsvi.1994.1184.

[7] Dahl, P. R., "Solid Friction Damping of Mechanical Vibrations," AIAA Journal, Vol. 14, No. 12, 1976, pp. 1675–1682.
doi: 10.2514/3.61511.

[8] Berger, E. J., and Krousgrill, C. M., "On Friction Damping Modeling Using Bilinear Hysteresis Elements," Journal of Vibration and Acoustics, Vol. 124, No. 3, 2002, p. 367.
doi: 10.1115/1.1473831.

[9] Kasai, T., and Link, M., "Identification of Non-Proportional Modal Damping Matrix and Real Normal Modes," Mechanical Systems and Signal Processing, Vol. 16, No. 6, 2002, pp. 921–934.
doi: 10.1006/mssp.2001.1478.

[10] Hanagud, S., Meyyappa, M., Cheng, Y. P., and Craig, J. I., "Identification of structural dynamic systems with nonproportional damping," AIAA Journal, Vol. 24, No. 11, Nov. 1986, pp. 1880–1882.
doi: 10.2514/3.9543.

[11] Balmes, E., "New Results on the Identification of Normal Modes From Experimental Complex Modes," Mechanical Systems and Signal Processing, Vol. 11, No. 2, Mar. 1997, pp. 229–243.
doi: 10.1006/mssp.1996.0058.

[12] Bi, S., Ouisse, M., Foltête, E., and Jund, A., "Virtual decoupling of vibroacoustical systems," Journal of Sound and Vibration, Vol. 401, 2017, pp. 169–189.
doi: 10.1016/j.jsv.2017.04.040.

[13] Pradhan, S., and Modak, S. V., "A method for damping matrix identification using frequency response data," Mechanical Systems and Signal Processing, Vol. 33, Nov. 2012, pp. 69–82.
doi: 10.1016/j.ymssp.2012.07.002.

[14] Arora, V., "Direct structural damping identification method using complex FRFs," Journal of Sound and Vibration, Vol. 339, Mar. 2015, pp. 304–323.
doi: 10.1016/j.jsv.2014.08.040.

[15] Adhikari, S., "On the quantification of damping model uncertainty," Journal of Sound and Vibration, Vol. 306, No. 1–2, 2007, pp. 153–171.
doi: 10.1016/j.jsv.2007.05.022.

[16] Koruk, H., and Sanliturk, K. Y., "Damping uncertainty due to noise and exponential windowing," Journal of Sound and Vibration, Vol. 330, No. 23, 2011, pp. 5690–5706.
doi: 10.1016/j.jsv.2011.07.006.

[17] Ouisse, M., and Foltête, E., "On the properness condition for modal analysis of non-symmetric second-order systems," Mechanical Systems and Signal Processing, Vol. 25, No. 2, Feb. 2011, pp. 601–620.
doi: 10.1016/j.ymssp.2010.08.017.

[18] Ouisse, M., and Foltête, E., "Model correlation and identification of experimental reduced models in vibroacoustical modal analysis," Journal of Sound and Vibration, Vol. 342, Apr. 2015, pp. 200–217.
doi: 10.1016/j.jsv.2014.12.042.

[19] Bi, S., Prabhu, S., Cogan, S., and Atamturktur, S., "Uncertainty Quantification Metrics with Varying Statistical Information in Model Calibration and Validation," AIAA Journal, Vol. 55, No. 10, 2017, pp. 3570–3583.
doi: 10.2514/1.J055733.

[20] Badcock, K. J., Timme, S., Marques, S., Khodaparast, H., Prandina, M., Mottershead, J. E., Swift, A., Da Ronch, A., and Woodgate, M. A., "Transonic aeroelastic simulation for instability searches and uncertainty analysis," Progress in Aerospace Sciences, Vol. 47, No. 5, 2011, pp. 392–423.
doi: 10.1016/j.paerosci.2011.05.002.

[21] Patelli, E., Govers, Y., Broggi, M., Gomes, H. M., Link, M., and Mottershead, J. E., "Sensitivity or Bayesian model updating: a comparison of techniques using the DLR AIRMOD test data," Archive of Applied Mechanics, Vol. 87, No. 5, 2017, pp. 905–925.
doi: 10.1007/s00419-017-1233-1.

[22] ASME V&V 10.1-2012, "An Illustration of the Concepts of Verification and Validation in Computational Solid Mechanics," 2012.

[23] Dascotte, E., and Strobbe, J., "Updating finite element models using FRF correlation functions," Proceedings of the 17th International Model Analysis Conference, 1999, pp. 1–6.

[24] Allemang, R. J., "The modal assurance criterion: twenty years of use and abuse," Sound and vibration, Vol. 8, 2003, pp. 14–21.

[25] Winter, G., Periaux, J., Galan, M., and Cuesta, P., Genetic Algorithms in Engineering and Computer Science, John Wiley & Sons, Inc., 1996.

[26] Zhang, Y., "Solving large-scale linear programs by interior-point methods under the Matlab Environment," Optimization Methods and Software, Vol. 10, No. 1, 1998, pp. 1–31.
doi: 10.1080/10556789808805699.

[27] Venter, G., and Sobieszczanski-Sobieski, J., "Particle Swarm Optimization," AIAA Journal, Vol. 41, No. 8, Aug. 2003, pp. 1583–1589.
doi: 10.2514/2.2111.

[28] Luo, Y.-Z., and Tang, G.-J., "Parallel Simulated Annealing Using Simplex Method," AIAA Journal, Vol. 44, No. 12, Dec. 2006, pp. 3143–3146.
doi: 10.2514/1.16778.